Supplementary Information:
Isotope-dependent site occupation of hydrogen in epitaxial titanium hydride nanofilms

T. Ozawa[1*], Y. Sugisawa[2], Y. Komatsu[3], R. Shimizu[3,4], T. Hitosugi[3,4], D. Sekiba[2], K. Yamauchi[5, †], I. Hamada[5], K. Fukutani[1,6]

[1]*Institute of Industrial Science, The University of Tokyo, Komaba, Meguro, Tokyo 153-8505, Japan*

[2]*Graduate School of Pure and Applied Sciences, University of Tsukuba, Tsukuba, Ibaraki 305-8573, Japan*

[3]*School of Materials and Chemical Technology, Institute of Science Tokyo, Ookayama, Meguro, Tokyo 152-8552, Japan*

[4]*Department of Chemistry, The University of Tokyo, Hongo, Bunkyo, Tokyo 113-0033, Japan*

[5]*Department of Precision Engineering, Graduate School of Engineering, Osaka University, Yamadaoka, Suita, Osaka 565-0871, Japan*

[6]*Advanced Science Research Center, Japan Atomic Energy Agency (JAEA), Shirakata, Tokai, Ibaraki 319-1195, Japan*

Supplementary Figures 1 –13

Supplementary Tables 1 –2

———————————————————

*Corresponding author. E-mail: t-ozawa@iis.u-tokyo.ac.jp

[†]Present address: *Center for Spintronics Research Network, Osaka University, 1-3 Machikaneyama, Toyonaka, Osaka 560-8531, Japan*

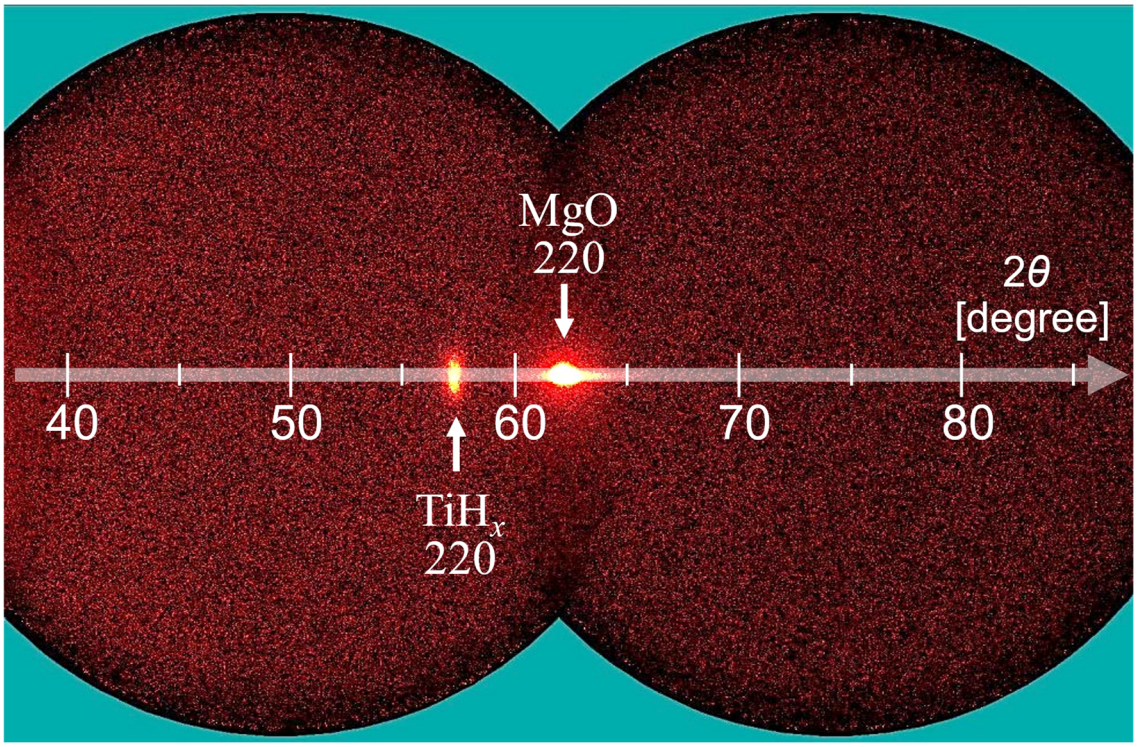

Supplementary Fig. 1 Two-dimensional x-ray diffraction (XRD) pattern for the 90-nm-thick $TiH_{1.47}$(110)/MgO(110) obtained by CuKα (λ = 1.5418 Å).

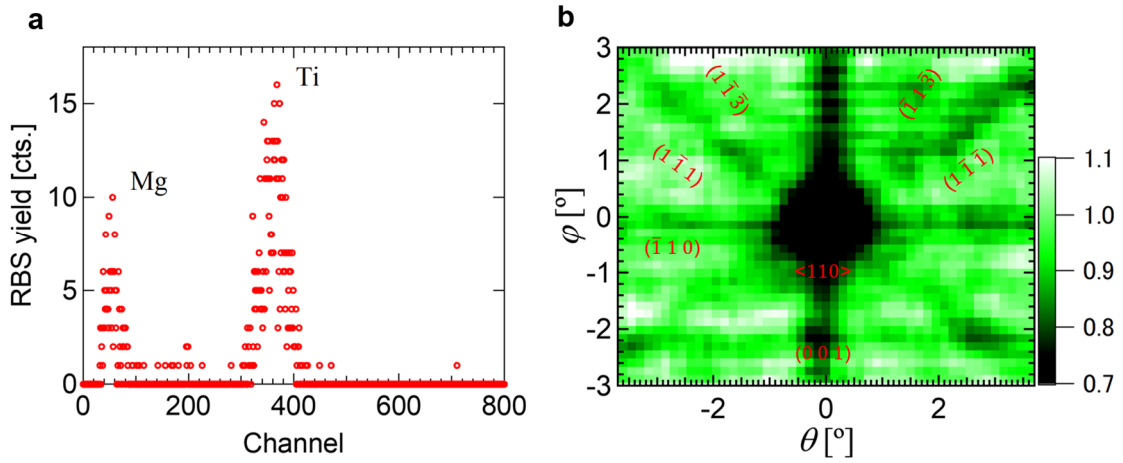

Supplementary Fig. 2 a RBS spectrum obtained by $^{15}N^{2+}$ beam with an energy of 6.45 MeV for the 90-nm-thick $TiH_{1.47}$(110)/MgO(110). **b** Two-dimensional (2D) angular mapping of the normalized Mg-RBS around the normal incidence.

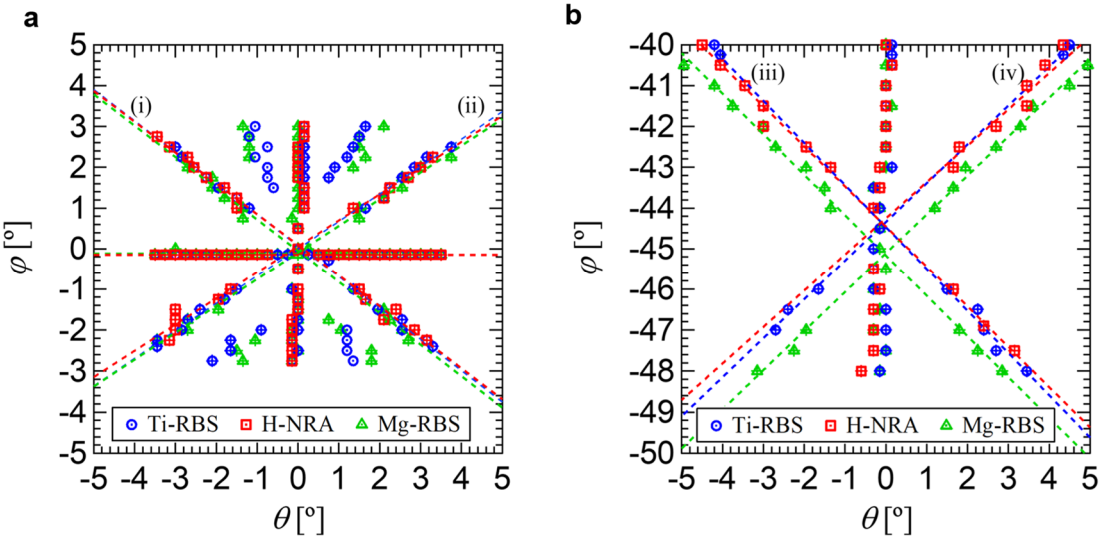

Supplementary Fig. 3 a, b Dip or peak positions extracted from the 2D mapping data of Ti-RBS, H-NRA, and Mg-RBS around the (**a**) <110> and (**b**) <100> directions for the $TiH_{1.47}$(110) film. Dotted lines represent linear fittings for the Ti-RBS (blue circle), H-NRA (red square), and Mg-RBS (green triangle).

Lines of (i) and (ii) around <110> in Supplementary Fig. 3						Planes of $[1\bar{1}\bar{1}]$ and $[1\bar{1}1]$ in cubic	
Ti-RBS		H-NRA		Mg-RBS			
angle [°]	intersection [°]	angle [°]	intersection [°]	angle [°]	intersection [°]	angle [°]	intersection [°]
71.3	(0.1,0.0)	69.6	(0.0,0.1)	70.8	(0.0,-0.1)	70.5	(0,0)

Lines of (iii) and (iv) around <100> in Supplementary Fig. 3						Planes of $[01\bar{1}]$ and $[1\bar{1}1]$ in cubic	
Ti-RBS		H-NRA		Mg-RBS			
angle [°]	intersection [°]	angle [°]	intersection [°]	angle [°]	intersection [°]	angle [°]	intersection [°]
89.4	(0.0,-44.3)	89.3	(0.0,-44.5)	88.4	(0.0,-45.1)	90.0	(0.0,-45.0)

Supplementary Table 1 Angles between the fitting lines of (i)-(ii) and (iii)-(iv), and their points of intersections. Those for an ideal cubic crystal are also listed. The fitting lines labeled (i)-(iv) are shown in Supplementary Fig. 3. Channeling experiments in different incident directions allow for evaluation of the lattice distortion. The observed angle between the <110> and <100> axes is smaller than 45.0° expected for the cubic structure, indicating an out-of-plane expansion of the $TiH_{1.47}$ epitaxial film. This is consistent with the XRD results in Fig. 1c and Supplementary Fig. 1 and a previous study[1] indicating the compressive epitaxial growth on the MgO(110) substrate.

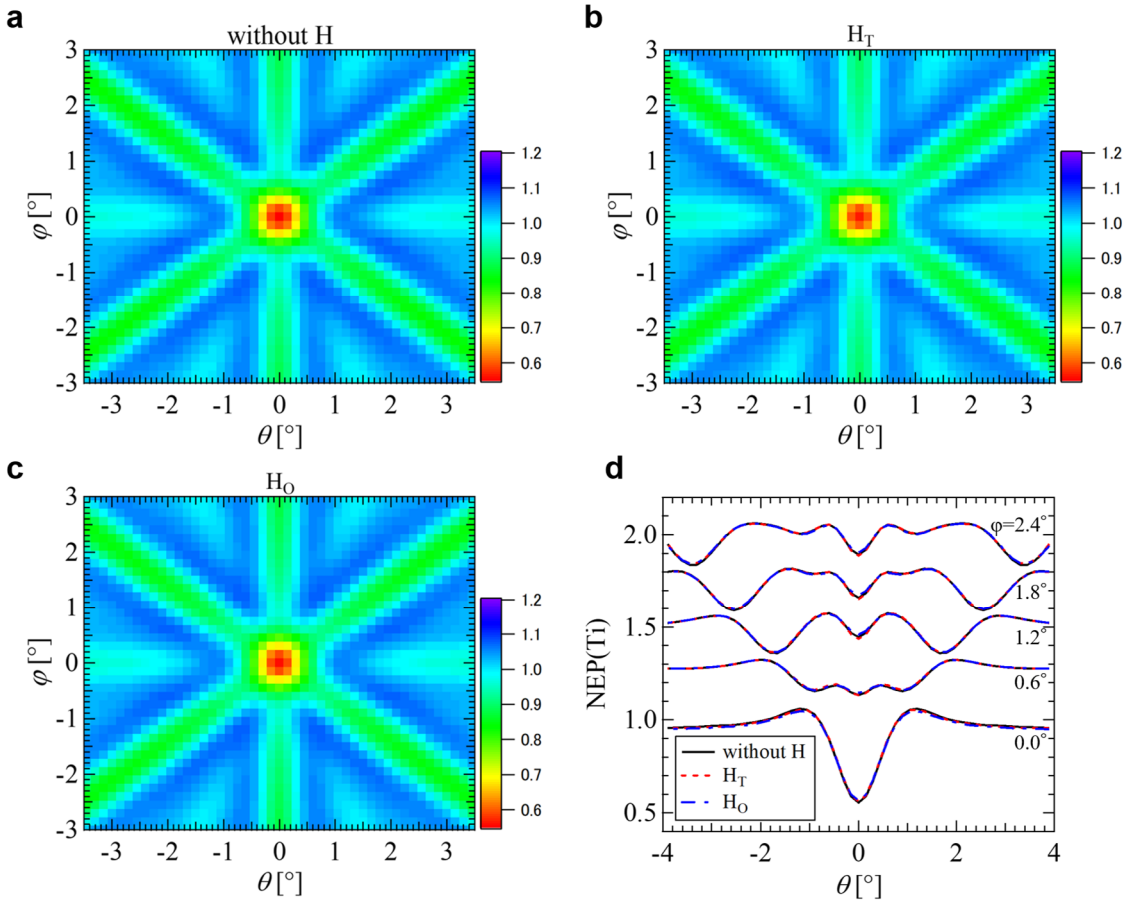

Supplementary Fig. 4 a-c 2D mappings of the nuclear close-encounter probabilities for Ti (NEP(Ti)'s) calculated for the structures (**a**) without H, (**b**) with H in the T site, and (**c**) with H in the O site. Vibrational amplitudes used in the calculations were 0.36, 0.25 and 0.45 Å for Ti, H in the T site, and H in the O site, respectively, and the beam divergence was assumed to be 0.25° for the $^{15}N^{2+}$ incident beam with an energy of 6.45 MeV. **d** Corresponding line profiles as a function of θ at various ϕ's.

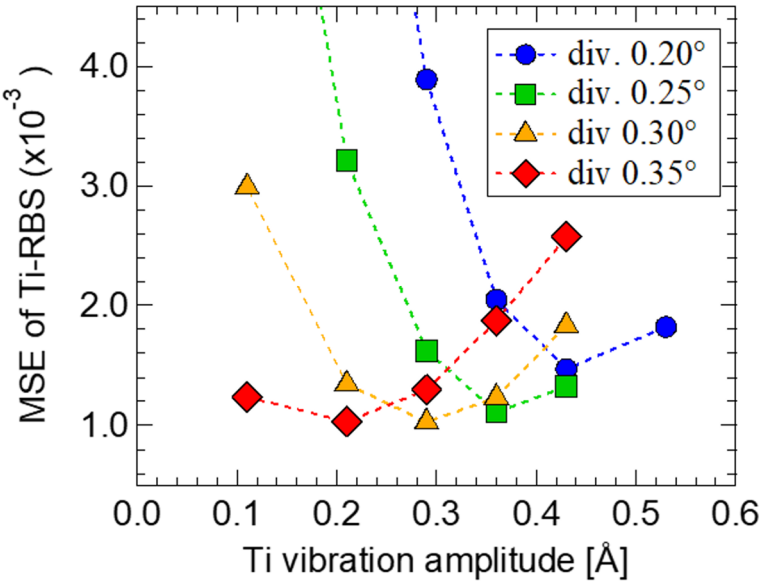

Supplementary Fig. 5 Mean squared error (MSE) as a function of the Ti vibrational amplitude between the 2D mappings of the normalized Ti-RBS obtained by $^{15}N^{2+}$ beam at an energy of 6.45 MeV around the normal incidence for the $TiH_{1.47}$(110) film and the NEP(Ti)'s of various beam divergence conditions. The MSE's were derived within the restricted ranges of θ = -3.45 ~ -1.50° and 1.50 ~ 3.45° and ϕ = 1.50 ~ 2.70° to avoid the blocking effect.

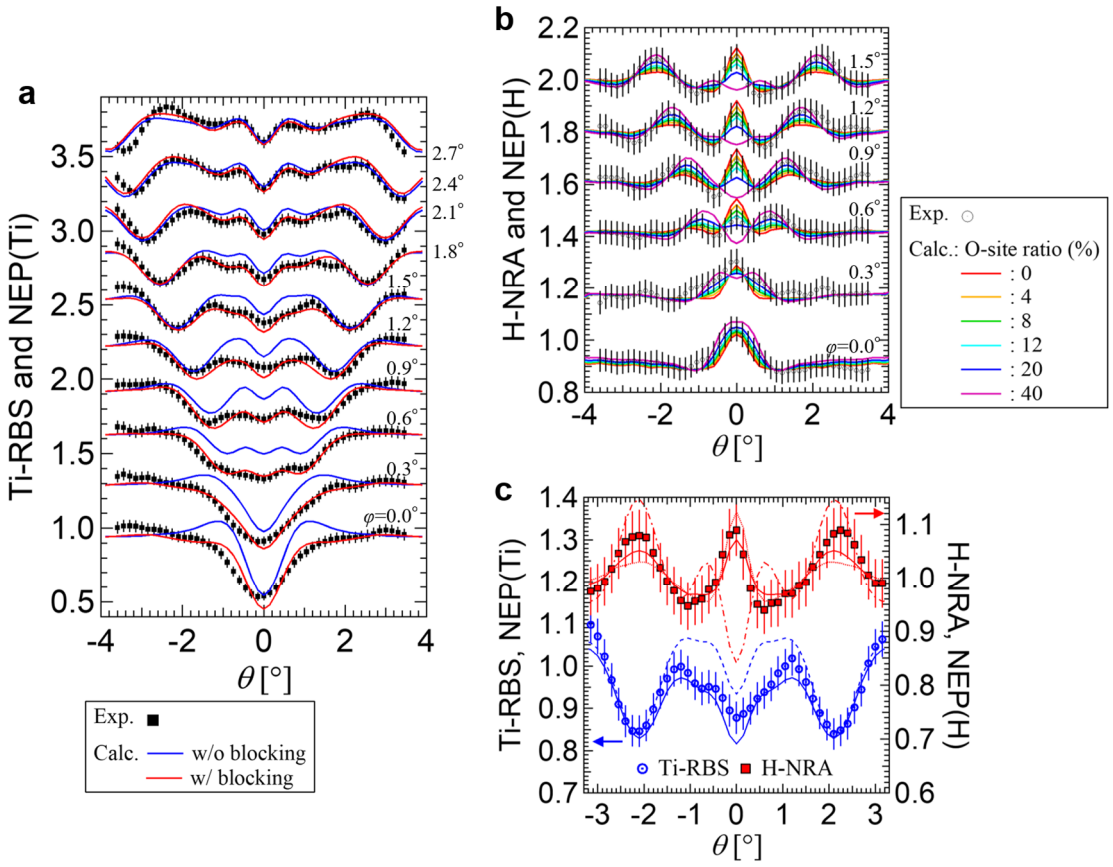

Supplementary Fig. 6 a Horizontal line scan profiles of the normalized Ti-RBS (dot) obtained by $^{15}N^{2+}$ beam at an energy of 6.45 MeV around the normal incidence for the $TiH_{1.47}$(110) film. The NEP(Ti) and the corr.-NEP(Ti) are also shown by blue and red solid lines, respectively. The corr.-NEP(Ti) represents the NEP(Ti) corrected by the blocking effect. **b** The horizontal line scan profiles of the normalized H-NRA (circle). NEP(H_T+H_O) (weighted average of NEP(H_T) and NEP(H_O)) with various O-site occupation ratios are also shown by solid lines. **c** Horizontal line scan profiles at ϕ=1.5° of the normalized Ti-RBS (circle) and the normalized H-NRA (square). The NEP(Ti) and the corr.-NEP(Ti) are represented by blue dotted and solid lines, respectively, and the NEP(H_T), NEP(Ho), and NEP(H_T+H_O) are shown by red dotted, dash-dotted, and solid lines, respectively. The beam divergence, the Ti vibration amplitude, and the H vibrational amplitudes for T and O sites were assumed to be 0.25°, 0.36 Å, 0.25Å, and 0.45Å in the calculations, respectively, and the NEP(H_T+H_O) assumed the O-site occupation by H at 10 at.%. The error bars in the experimental data represent the statistical uncertainty.

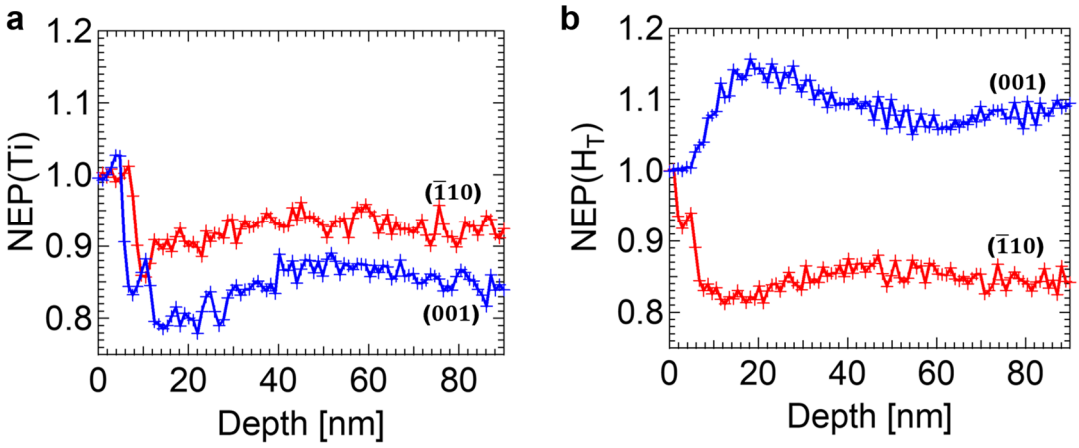

Supplementary Fig. 7 a, b Depth dependence of the calculated (**a**) NEP(Ti) and (**b**) NEP(H_T) at (001) and ($\bar{1}$10) plane channeling conditions for the structure with H in the T site assuming the $^{15}N^{2+}$ beam with an incident energy of 6.45 MeV.

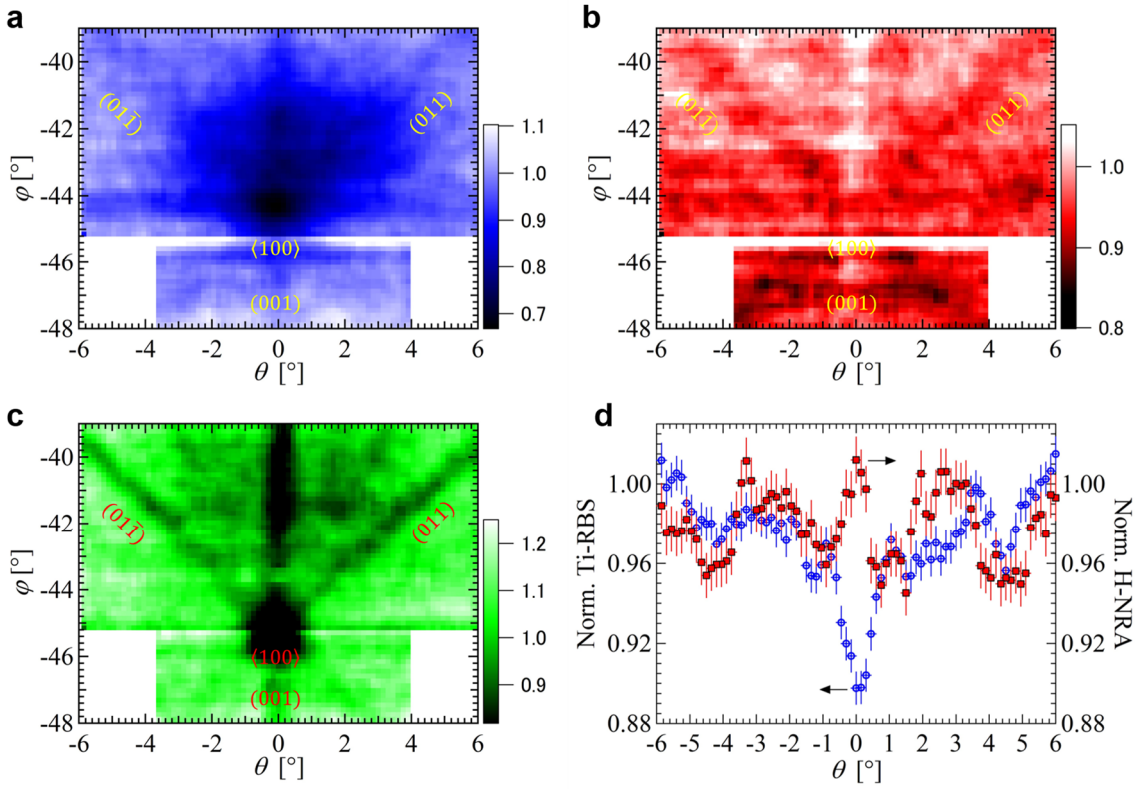

Supplementary Fig. 8 a-c Two-dimensional mappings of the normalized (**a**) Ti-RBS, (**b**) H-NRA, and (**c**) Mg-RBS as functions of θ and ϕ around the <100> direction by oblique incidence measured by $^{15}N^{2+}$ beam with an energy of 6.50 MeV for the $TiH_{1.47}$(110) film, which corresponds to a H probing depth of ~30 nm from the surface. **d** Horizontal line scan profiles of the Ti-RBS and H-NRA at ϕ = -40.0°. The error bars represent the statistical uncertainty. The angle between the <110> and <100> axes observed in the Ti-RBS was derived to be 44.3°, which is smaller than 45.0° expected for the cubic structure, indicating an average out-of-plane expansion of the $TiH_{1.47}$ epitaxial film by 1.2 %. It is noted that both Ti-RBS and H-NRA mappings at the oblique incidence were blurred and their intensity changes under the channelings are smaller than those of the normal incidence. This implied that the crystallographic direction is randomly inclined around the surface normal direction, as is also confirmed by the slightly broad XRD rocking curve, resulting in the smaller channeling effect. Because the oblique incident experiment was performed after the normal incident experiment, the sample aging due to the ion beam irradiation also negatively affected the channeling effect.

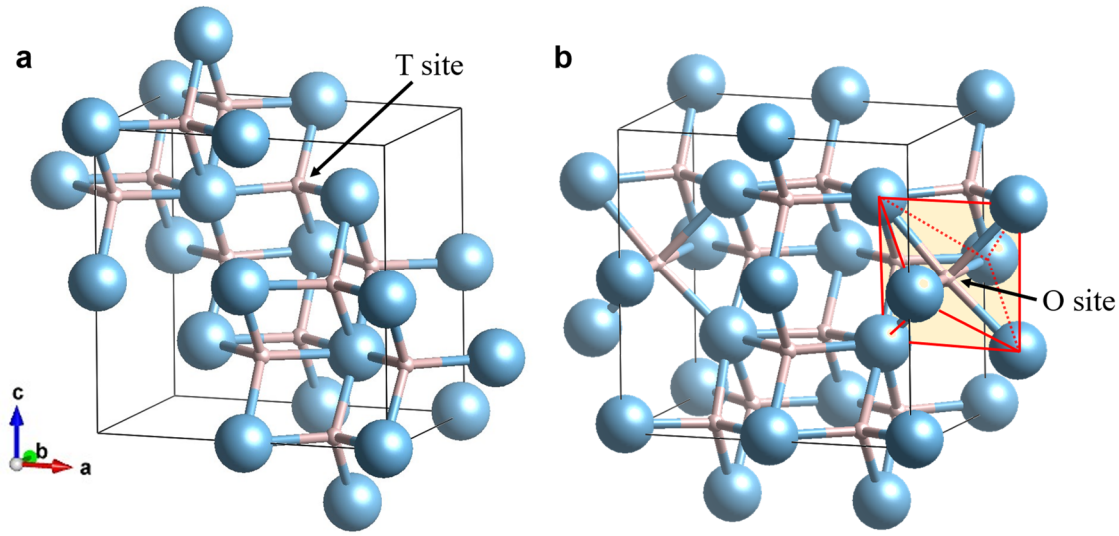

Supplementary Fig. 9 a, b The lowest energy configurations of Ti_8H_{12} obtained by the DFT calculations for (**a**) 12T and (**b**) 11T1O structures. Blue and pink circles represent Ti and H atoms, respectively. The H migration energy from T to O sites was calculated to be 439 (432) meV with (without) the ZPE. The average displacements for Ti atoms are 0.07±0.03 Å and 0.23±0.05 Å in (**a**) the 12T and (**b**) the 11T1O structures, respectively. The symmetry of the crystal structure is lowered from *Fm-3m* at 16T to *Pm* at the 11T1O. Furthermore, the local symmetry at the Ti sites is also lowered from *m-3m* to either 1 or *m*. These symmetry lowering lifts the orbital degeneracy of the Ti-*3d* states. Corresponding total DOS's and projected DOS's for Ti 3d are shown in Fig. 6 in the main text.

ZPE (eV/s.c.)	12T	11T1O
H	3.077	2.984
D	2.270	2.202

Supplementary Table 2 Calculated total ZPEs (eV/s.c.) for the lowest-energy 12T and 11T1O configurations. The ZPE difference between the 12T and 11T1O configurations was estimated to be 93 (67) meV for H (D). These values are adapted in the main text.

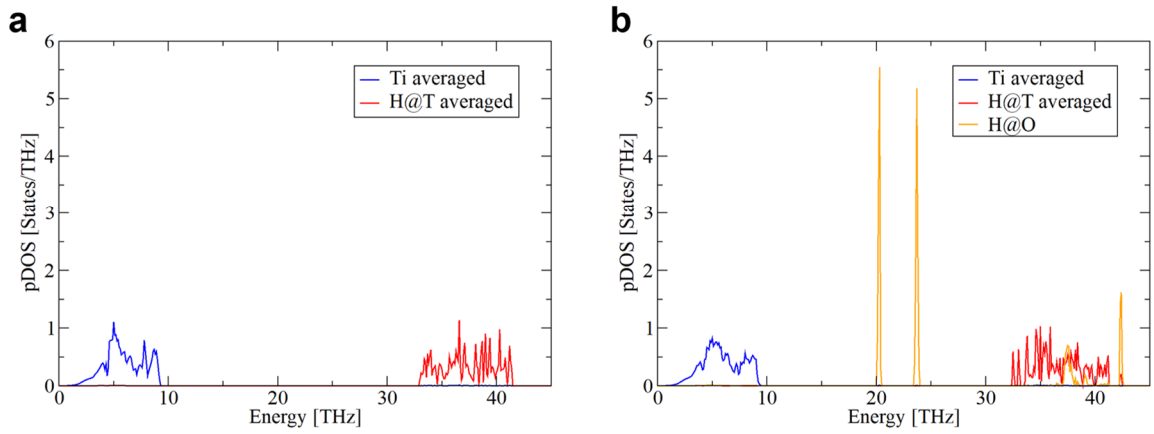

Supplementary Fig. 10 a, b Projected density of states [pDOS, $\rho(E)$] for phonon obtained by the DFT calculations for the lowest-energy (**a**) 12T and (**b**) 11T1O configurations. Those onto Ti atoms, H atoms at the T site (H@T), and H atoms at the O site (H@O) are shown. For Ti and H@T, the average pDOSs are shown. We calculated the ZPE for each atom by integrating $\frac{1}{2} E \rho(E)$ to obtain 39 and 228 meV for Ti and H@T in the 12T structure [(**a**)], respectively, and 39, 223, and 160 meV for Ti, H@T, and H@O in the 11T1O structure [(**b**)], respectively. When H is replaced with D, the corresponding ZPEs were calculated to be 40 and 156 for Ti and D@T, respectively, in the 12T structure, and 40, 160, and 117 meV for Ti, D@T, and D@O, respectively, in the 11T1O structure. These are consistent with the result shown in Supplementary Table 2.

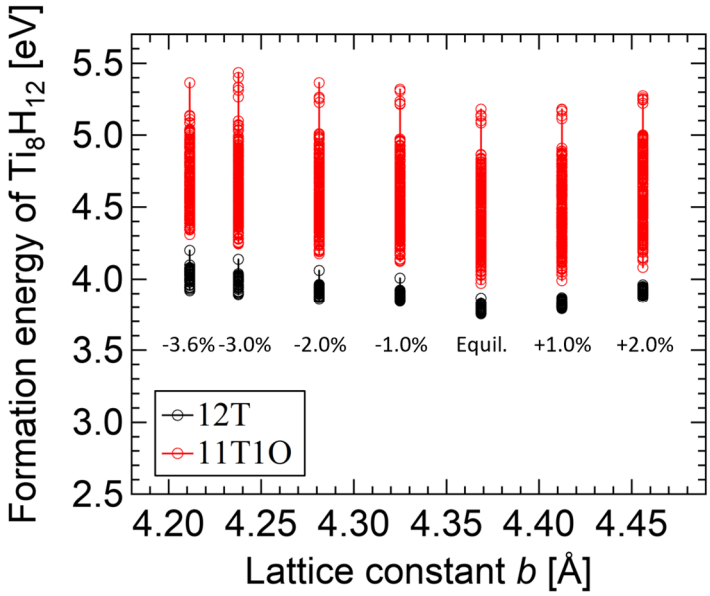

Supplementary Fig. 11 Formation energies of Ti_8H_{12} as a function of lattice constant *b* for 12T and 11T1O structures obtained by the DFT calculations by tuning the basal lattice constants *a* and *b*, where *a* is given as $\sqrt{2}b$. The *c* length was optimized to keep the cell volume constant at the given *a* and *b* parameters. The lattice constant of -3.6% compression corresponds to that of the MgO(110) substrate.

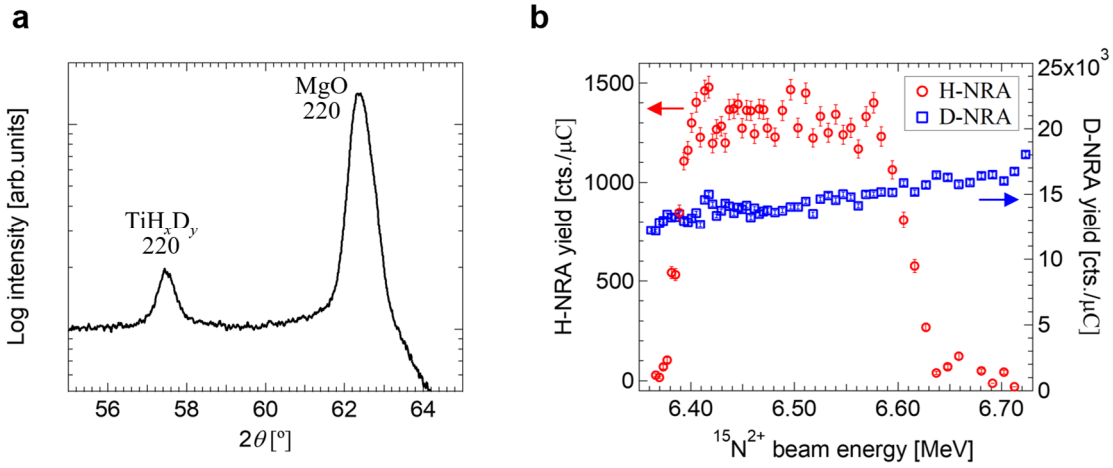

Supplementary Fig. 12 a, b (**a**) Out-of-plane θ-2θ XRD pattern obtained by CuKα (λ = 1.5418 Å) and (**b**) H- and D-NRA profiles at random incidence for the 100-nm-thick $TiH_{0.60}D_{1.0}$(110)/MgO(110). The error bars represent the statistical uncertainty. The normalization constant for the H,D-NRA is different from that shown in Fig. 1e in the main text.

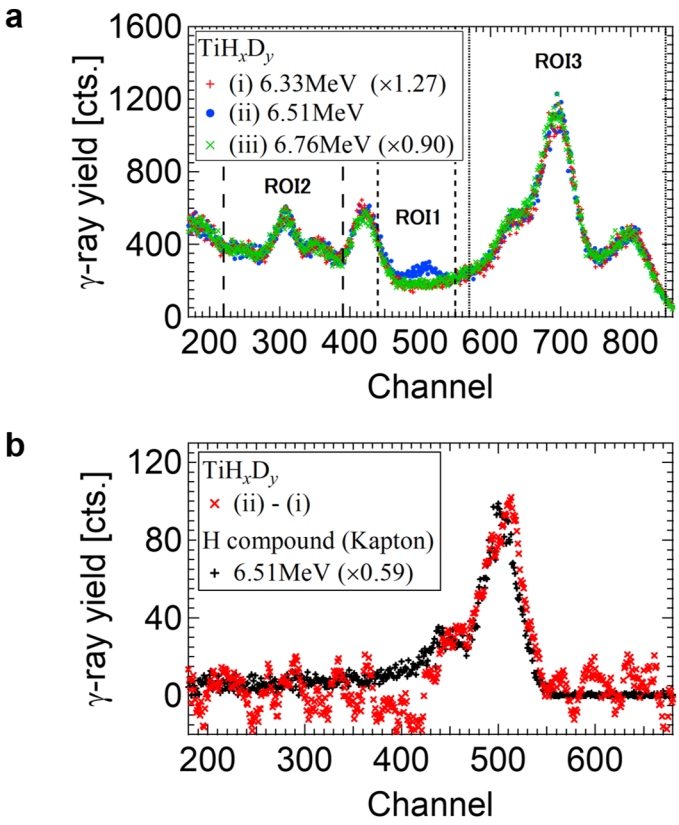

Supplementary Fig. 13 a γ-ray spectra observed by $^{15}N^{2+}$ beam with incident energies of (i) 6.33, (ii) 6.51, and (iii) 6.76 MeV for the $TiH_{0.60}D_{1.0}$(110) film. Since the incident energies at (i) and (iii) are out-of-resonance of the nuclear reaction with H, the γ-ray yields at (i) and (iii) solely reflect the contribution of those with D. The γ-ray yield at (ii) consists of the two contributions of H and D. Data scales are adjusted depending on the incident energies. **b** Subtraction of the γ-ray yields at energies of (ii) 6.51 MeV (within the resonance for H) and (i) 6.33 MeV (out-of-resonance), which basically represents the contribution of H. The data is a 10-point moving average. The spectrum for a H compound (Kapton foil) at an energy of 6.51 MeV is also shown for reference, which is consistent with the subtraction spectrum, showing that the γ-ray yield of H can be extracted by subtracting the contribution of D. Since the ratio of the γ-ray yields of D at ROI1 and ROI(2+3) is almost constant independent of the incident energy as shown by the spectra for (i) and (iii) in (**a**), the γ-ray yield of H is derived by subtracting a constant multiple of the yield at ROI(2+3) from that at ROI1.

Supplementary References

1. Shimizu, R. *et al.* Polarity reversal of the charge carrier in tetragonal TiHx (x =1.6−2.0) at low temperatures. *Phys. Rev. Res.* **2**, 033467 (2020).